ACS APPLIED MATERIALS & INTERFACES

Research Article

www.acsami.org

Low-Temperature Solution-Processed Kesterite Solar Cell Based on in Situ Deposition of Ultrathin Absorber Layer

Yi Hou,[*,†,§] Hamed Azimi,[*,†] Nicola Gasparini,[†] Michael Salvador,[†,⊥] Wei Chen,[†,§] Laraib S. Khanzada,[†,#] Marco Brandl,[∥] Rainer Hock,[∥] and Christoph J. Brabec[†,‡]

[†]Institute of Materials for Electronics and Energy Technology (I-MEET), Department of Materials Science and Engineering, Friedrich-Alexander University Erlangen-Nuremberg, Martensstrasse 7, 91058 Erlangen, Germany

[‡]Bavarian Center for Applied Energy Research (ZAE Bayern), Haberstrasse 2a, 91058 Erlangen, Germany

[§]Erlangen Graduate School in Advanced Optical Technologies (SAOT), Paul-Gordan-Strasse 6, 91052 Erlangen, Germany

[∥]Chair for Crystallography and Structural Physics, Friedrich-Alexander-University Erlangen-Nürnberg, Staudtstrasse 3, 91058 Erlangen, Germany

[⊥]Instituto de Telecomunicações, Instituto Superior Técnico, Av. RoviscoPais, P-1049-001 Lisboa, Portugal

[#]Department of Metallurgical Engineering, NED University of Engineering and Technology, University Road, Karachi 75270, Pakistan

Supporting Information

ABSTRACT: The production of high-performance, solution-processed kesterite $Cu_2ZnSn(S_xSe_{1-x})_4$ (CZTSSe) solar cells typically relies on high-temperature crystallization processes in chalcogen-containing atmosphere and often on the use of environmentally harmful solvents, which could hinder the widespread adoption of this technology. We report a method for processing selenium free Cu_2ZnSnS_4 (CZTS) solar cells based on a short annealing step at temperatures as low as 350 °C using a molecular based precursor, fully avoiding highly toxic solvents and high-temperature sulfurization. We show that a simple device structure consisting of ITO/CZTS/CdS/Al and comprising an extremely thin absorber layer (~110 nm) achieves a current density of 8.6 mA/cm^2. Over the course of 400 days under ambient conditions encapsulated devices retain close to 100% of their original efficiency. Using impedance spectroscopy and photoinduced charge carrier extraction by linearly increasing voltage (photo-CELIV), we demonstrate that reduced charge carrier mobility is one limiting parameter of low-temperature CZTS photovoltaics. These results may inform less energy demanding strategies for the production of CZTS optoelectronic layers compatible with large-scale processing techniques.

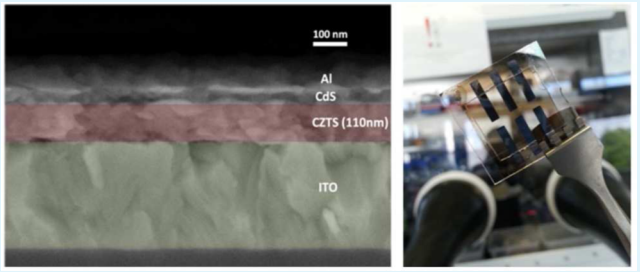

KEYWORDS: *CZTS, kesterite solar cells, molecular based precursor, low-temperature processing, device stability*

INTRODUCTION

Solution-processed inorganic semiconductors exhibit a broad range of attractive optoelectronic properties, and hold great promise for enabling inexpensive and large area roll-to-roll device fabrication.[1,2] Recently, low-temperature, solution-processed nanocrystalline inorganic and hybrid semiconductors, based on earth-abundant elements, have attracted broad attention.[3−6] Among these classes of materials, Pb based semiconductors such as PbS and inorganic−organic Pb based perovskites, demonstrated record high efficiencies of 8.6% and 20.1%, respectively.[5,6] However, multistep photovoltaic device fabrication, sometimes including complicated ligand exchange protocols, and concerns regarding the toxicity and the limited lifetime of these absorber materials may represent important hurdles when considering large-area deployment of these materials. Conversely, semiconductors based on environmentally benign, largely available materials like FeS_2, Cu_2O, and $Cu_2ZnSn(S_xSe_{1-x})_4$ (CZTSSe) open up opportunities for large-scale photovoltaic implementation.[3,4,7,8] Particularly, the case of CZTSSe has regained significant interest through reports of high-efficiency solar cells based on molecular precursors and nanocrystal inks.[9−12] In theory, Cu_2ZnSnS_4 (CZTS) represents an optimum absorber material for solar cell mass production. It features p-type conductivity, an optimal direct band gap of ~1.5 eV, and a high absorption coefficient of ~10^4 cm^{-1}.[13] The latter suggests that devices with active layer thicknesses smaller than the typically employed 1−2 μm could function efficiently.

High-performance CZTSSe devices with power conversion efficiencies (PCEs) of up to 12.6% rely on high-temperature

Received: May 22, 2015
Accepted: September 10, 2015
Published: September 10, 2015

DOI: 10.1021/acsami.5b04468
ACS Appl. Mater. Interfaces 2015, 7, 21100−21106

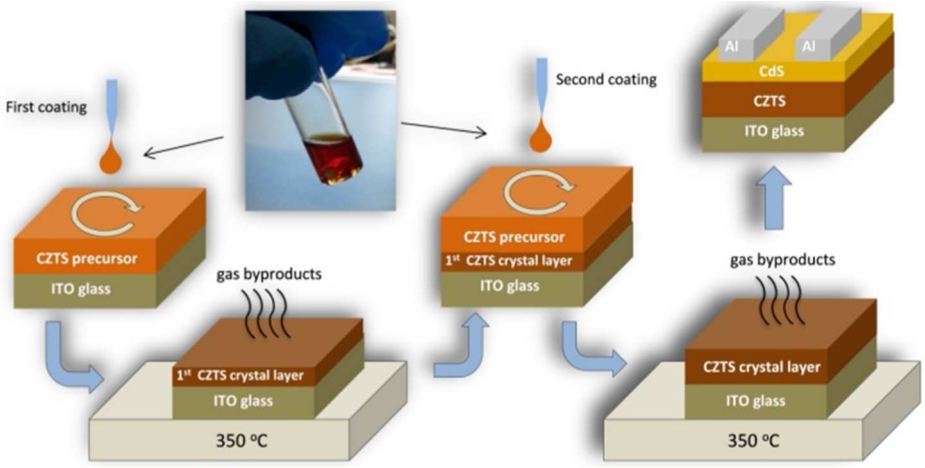

Figure 1. Scheme representing the fabrication of low-temperature processed CZTS solar cells. After stirring the precursor solution for ∼10 min, precursor films were directly spin coated on ITO coated glass substrates and subsequently annealed at 350 °C for 5 min on a hot plate inside a glovebox. Following the formation of the first layer, a second CZTS layer was deposited on top of the first layer and annealed at the same temperature for an additional time of 2 min. All devices were finalized by depositing a ∼ 30 nm thick precursor based CdS layer and an 80 nm aluminum top electrode.

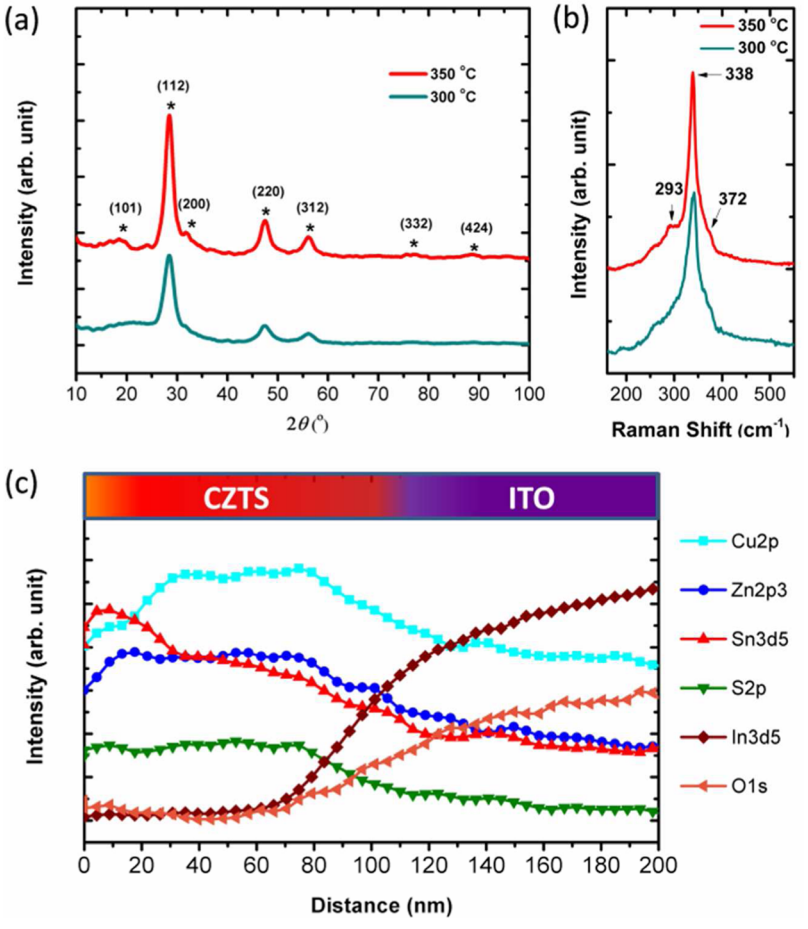

Figure 2. (a) XRD diffraction patterns of as-synthesized CZTS films after thermal annealing at 300 and 350 °C for 5 min; (b) Raman spectra of the CZTS films annealed at 300 and 350 °C for 5 min; (c) XPS depth profile of a ∼100 nm CZTS film deposited on an ITO coated glass substrate and annealed at 350 °C for 5 min.

annealing (∼500 °C) under chalcogen atmosphere and/or hydrazine based methodologies. The high-temperature post-treatment and toxicity of hydrazine make these approaches rather incompatible with large-scale manufacturing standards. Korgel et al. previously reported on low-temperature processed CZTS solar cells based on spray coating of CZTS nanoparticles. The rather low conversion efficiency (0.23%) could have originated by long-chain organic ligands.[3] Talapin et al. recently described continuous films of high phase purity, organic-ligand-free CZTS using small inorganic ligands such as

DOI: 10.1021/acsami.5b04468
ACS Appl. Mater. Interfaces 2015, 7, 21100−21106

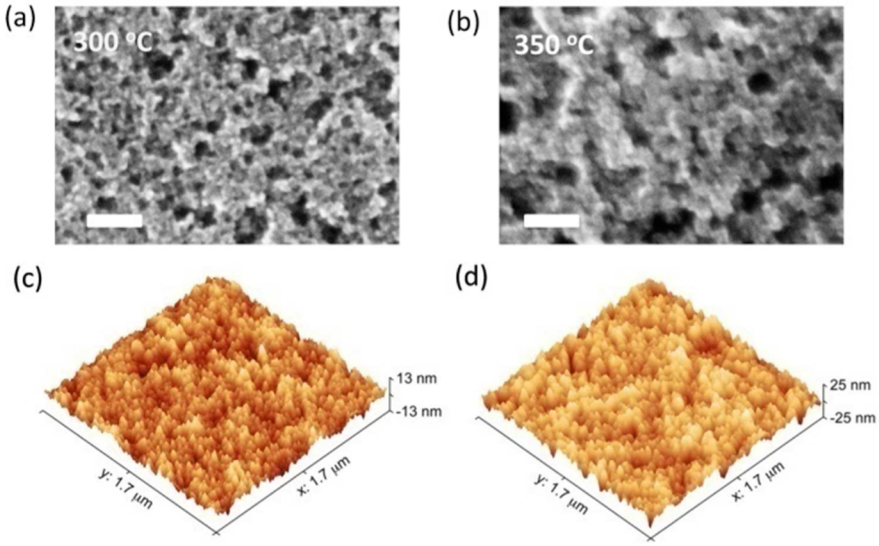

Figure 3. SEM and AFM images of molecular precursor CZTS films annealed at different temperatures: (a, b) top-view SEM images of CZTS films annealed for 5 min at 300 and 350 °C, respectively; (c, d) 3D renderings of AFM topography (intermittent contact) of the same films shown in parts a and b, respectively. The bars in the SEM images correspond to 50 nm.

molecular metal chalcogenide complexes instead, but no working devices were reported.[14] Generally, the major obstacle is that colloidal NCs are typically stabilized by bulky, insulating surface ligands, which could form energetic barriers between the NCs. These surface ligands not only may limit charge transport on the surface of the particles but also could produce film discontinuities under moderate annealing temperatures.[2,15,16]

Here, we report a low-temperature route for the fabrication of CZTS nanostructured solar cells using metallic salt precursors in dimethyl sulfoxide (DMSO) solution. For the fabrication of the active layer we adopted a relatively short annealing step, thereby still forming a kesterite phase, as demonstrated by chemical analysis. DMSO as a solvent for CZTS absorber layers has been used before although in combination with high (>500 °C) annealing temperatures.[8] The present method has the advantage of being ligand-free, allowing the fusion and amalgamation of CZTS nanoparticles at a relatively low annealing temperature of 350 °C, which could, in turn, facilitate charge transport throughout the active layer. This approach avoids highly toxic materials as a reactant or solvent as well as high-temperature post-treatment steps, thus providing an attractive route toward environmentally benign and scalable low-temperature solution-processed photovoltaics.

RESULTS AND DISCUSSION

The molecular based precursor solution was prepared using a mixture of different metal salts and thioacetamide (TAA) dissolved in DMSO. We found that the use of TAA instead of thiourea is particularly important for the formation of CZTS nanocrystals at relatively low temperatures. The experimental procedure is described in detail in the Supporting Information (SI). TAA was used as the source for sulfur, which can easily decompose during the annealing temperature applied here.[17] TAA is expected to minimize the amount of organic impurities in targeted CZTS films. The overall composition of the precursor solution was aimed to be copper poor and zinc rich, which follows previous reports on state-of-the-art CZTS solar cells.[18] The precursor solution was stirred until all solid components were fully dissolved (~10 min). During this process the color of the precursor solution turned from yellow to clear wine red (Figure 1). The precursor solution was spin coated on ITO coated glass substrates and subsequently annealed inside a glovebox. Within the first 5 s of a 5 min annealing step at 300 and 350 °C, the molecular precursor films quickly changed color from nearly colorless to light brown, suggesting that a chemical reaction and, specifically, the formation of CZTS occurred. The UV−vis absorption spectra of the resulting films taken at different annealing temperatures are shown in Supporting Information, Figure S1. The onset of absorption underwent a red shift with increasing annealing temperature, indicating the growth of the CZTS nanocrystals and a decrease of the band gap.

To confirm the formation of CZTS in our films, we performed X-ray diffraction (XRD). Figure 2a shows XRD patterns of as-synthesized CZTS films annealed at 300 and 350 °C. For a sample annealed at 350 °C, diffraction peaks observed at 2θ = 18.42°, 28.40°, 32.07°, 47.41°, 56.07°, 69.28°, 76.98°, and 88.72° can be indexed to the (101), (112), (200), (220), (312), (332), and (424) planes of the standard single kesterite phase (JCPDS no. 26-0575), suggesting the formation of the kesterite phase. Conversely, a sample annealed at 300 °C does not show the full range of diffraction peaks associated with the kesterite phase, implying a lower degree of crystallinity and purity. The formation of the kesterite phase is further verified by Raman measurements (Figure 2b). The films that were annealed at 350 °C exhibited Raman signals at 293, 338, and 372 cm^{-1} associated with the CZTS kesterite phase. The main peak at 338 cm^{-1} closely matches the values reported for bulk CZTS.[19−21] Notably, the shoulders at 293 and 372 cm^{-1} have also been assigned to identify the kesterite-type crystal structure. These weak shoulder peaks pick up intensity when increasing the temperature from 300 to 350 °C, further indicating the formation of a higher quality kesterite phase when increasing the temperature to 350 °C. On the basis of the Scherrer equation,[22] the average crystallite size (D) along (112)-plane orientation was calculated to increase from 3.7 to 4.8 nm upon enhancing the annealing temperature from 300 to 350 °C.

DOI: 10.1021/acsami.5b04468
ACS Appl. Mater. Interfaces 2015, 7, 21100−21106

We further investigated the compositional distribution of the constituting elements across the CZTS film using X-ray photoelectron spectroscopy (XPS) depth profile measurements. As depicted in Figure 2c, the CZTS film featured a relatively uniform compositional distribution at the middle of the absorber layer with some depletion of Cu and Zn and a slight enrichment of Sn close to the film surface, while no traces of undesired elements were found within the detection limit for XPS measurement (~0.1−1 atomic %). Due to the slight Sn enrichment on the film surface, the formation of phases like Cu_2SnS_3, SnS_2, and Sn_2S_3 cannot be excluded. Using energy dispersive X-ray analysis, the average composition of the CZTS film was determined to be Cu/(Zn + Sn) = 0.87, Zn/Sn = 1.1, corresponding to a slightly copper poor and zinc rich CZTS phase, which is within the range of compositions reported for high-performance CZTS solar cells.

The morphology of the CZTS thin films annealed at different temperatures was characterized by scanning electron (SEM) and atomic force microscopy (AFM) measurements. After annealing at 300 °C, a fine-grained CZTS layer comprising relatively small irregular domains of varying porosity was formed (Figure 3a,c). Increasing the annealing temperature to 350 °C resulted in a more compact and dense morphology (Figure 3b,d). This evolution of the morphology was accompanied by an increase in topographical roughness from 13 to 29 nm RMS, according to the AFM scans shown in Figure 3c,d. Notably, the morphology of the molecular precursor CZTS films presented here differs from previously reported examples of CZTS films fabricated from particulate based inks at low annealing temperatures.[3] Because in our approach there are no bulky organic ligands on the particle surface, we hypothesize that the nanoparticles are easily fused together, forming a well-connected mesoporous-type structure.

We adopted a simple photovoltaic device geometry consisting of ITO/CZTS/CdS/Al to probe the effect of CZTS absorber layer thickness on the device performance (see Figure 4 and Table 1). CdS was deposited on top of the CZTS layer using a precursor solution based approach (see experimental details in the SI). The thickness variation was obtained by spin coating of one, two, and three layers of CZTS, yielding absorber thicknesses of 70, 110, and 165 nm, respectively. Increasing the number of coatings from a single to a double layer enhanced the short circuit current density (J_{sc}) from 3.56 to 7.59 mA/cm^2, with no observable drop in FF. The increase in J_{sc} can be explained by stronger light absorption translating effectively into improved charge carrier photogeneration. Conversely, attempts to further increase the thickness of the photovoltaic absorber by adding a third layer did not result in a better photoresponse (Figure S3). Instead, the $I-V$ performance would feature a poor diode behavior with elevated leakage current. While in the light of the present results an increase of the absorber layer appears to be a viable route to further increase device performance, additional investigations are required and underway to understand the lack of photovoltaic response for thicker CZTS films.

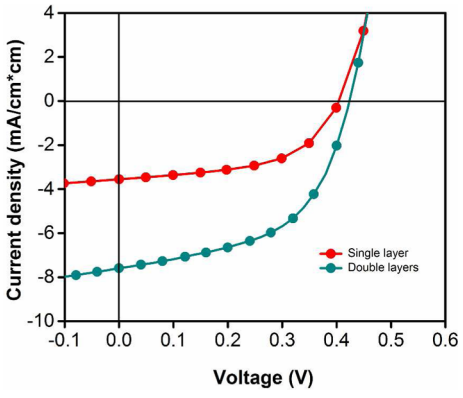

Figure 4. Current−voltage ($I-V$) characteristics of CZTS solar cells with different thicknesses, fabricated using single and double coatings. Solar cells were measured under 100 mW cm^{-2} AM1.5G illumination.

Table 1. Device Parameters for Solar Cells Prepared with Varying Thicknesses of the CZTS Layer

number of layers	J_{sc} [mA/cm^2]	V_{oc} [V]	FF [%]	eff [%]
single layer (~70 nm)	3.56	0.40	54.9	0.78
double layer (~110 nm)	7.59	0.42	53.1	1.71

The $I-V$ characteristics under AM1.5G solar simulator light (100 mW cm^{-2}) and the external quantum efficiency (EQE) response of a champion CZTS solar cell, in which case the active layer was annealed at 350 °C, are shown in Figure 5a,b (see the Supporting Information for a comparison between the performance of solar cells fabricated with different annealing recipes, Figure S2 and Table S1). The solar cell yielded a champion power conversion efficiency of 1.85% based on an open circuit voltage (V_{oc}) of 0.43 V, a short circuit current density of 8.57 mA/cm^2, and a fill factor (FF) of 49.9%. The measured J_{sc} represents close to 50% of the J_{sc} of state-of-the-art CZTS solar cells reported in the literature based on high-temperature sulfurization with an absorber thickness of ~600 nm.[18] The EQE measurement of the same device yielded a current density of J_{sc} 8.31 mA/cm^2, consistent with the $I-V$ measurement under 1-sun conditions. The low EQE signal in the range 600−850 nm can be attributed to incomplete light absorption due to the very thin absorber layer (110 nm). From the relationship $[E \times \ln(1 - \mathrm{EQE})]^2$ versus energy (E), the band gap of this low-temperature CZTS is determined to be 1.48 ± 0.03 eV, which is in line with previously reported values for kesterite CZTS thin films.[23] The relatively low EQE in the wavelength regime 300−500 nm can be attributed to parasitic absorption of the CdS buffer layer. Table 1 summarizes the photovoltaic device parameter of the solar cells studied in this work. The results of 30 solar cells showed that the average PCEs of our low-temperature processed CZTS solar cells reached about 1.5% (see Figure S4).

Interestingly, we also find that low-temperature processed glass-encapsulated CZTS solar cells (annealing temperature of 350 °C) show excellent stability. Photovoltaic device parameters and the resulting power conversion efficiency retain almost 100% of the initial value after 400 days of storage in air (Figure 5c).

We now return to the morphology of the CZTS layer. Figure 5d shows a cross-sectional SEM image of a complete solar cell fabricated by sintering at 350 °C. The SEM micrograph reveals a granular structure of the absorber layer. We assume that this porous, yet well-interconnected, nanostructure could have limiting implications on charge transport behavior, as discussed further below. In the past, there have been reports of efficient nanostructured solar cells composed of a porous matrix filled with a semiconductor of opposite doping.[24] We hypothesize that the degree of porosity present in our low-temperature, solution-processed CZTS films (Figure 2a,b) could potentially

DOI: 10.1021/acsami.5b04468
ACS Appl. Mater. Interfaces 2015, 7, 21100−21106

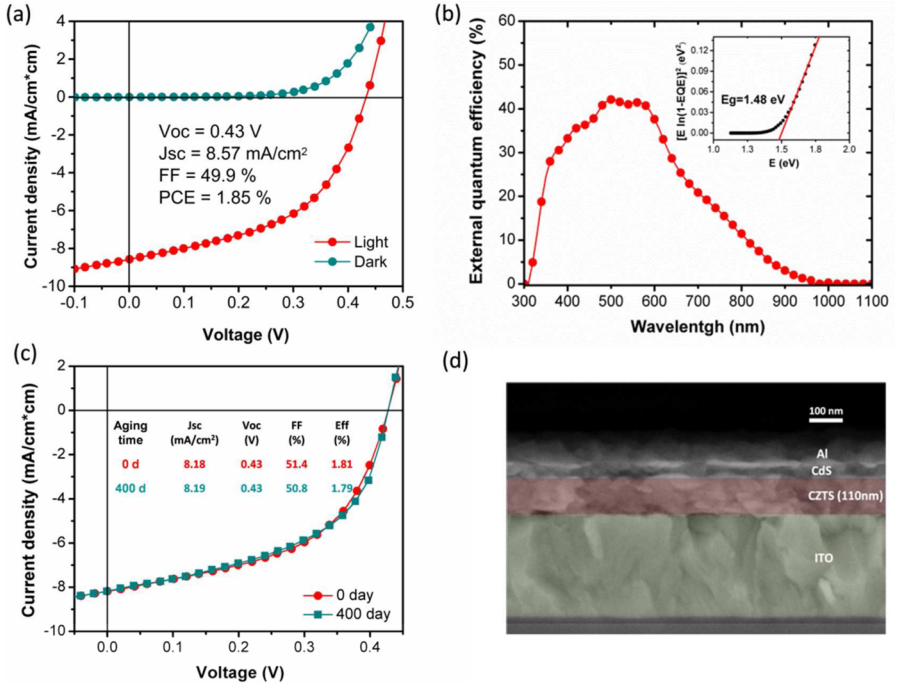

Figure 5. (a) $I-V$ characteristics measured under 100 mW cm^{-2} AM1.5G illumination (red line) and in the dark (blue line) for the best performing CZTS solar cell annealed at 350 °C. (b) External quantum efficiency (EQE) of the best performing device. The integrated short circuit current gives rise to 8.30 mA/cm^2. The band gap of the absorber layer was determined to be 1.48 eV by plotting $[E\ \ln(1 - \mathrm{EQE})]^{-2}$ versus E, as shown in the inset of part b. (c) Comparison of device performance for a solar cell before and after 400 days of aging in air. (d) Cross-sectional SEM micrograph of a device with the structure glass/ITO/CZTS (110 nm)/CdS(30 nm)/Al(80 nm).

benefit the formation of such an interpenetrating bulk heterojunction network when combined with an n-type semiconductor, possibly overcoming the limitation of poor carrier collection.

To gain insight into the charge transport behavior of this type of device we used impedance spectroscopy, an effective method that allows characterization of semiconductor properties. This technique has been shown to be particularly useful for measuring charge carrier lifetime as well as mobility of charge carriers in semiconductor materials.[25−27] Here, impedance spectra were taken in the dark by superimposing an harmonic voltage modulation (ac amplitude of 20 mV) and a dc bias of 400 mV. A representative impedance spectrum for the investigated cells is displayed in Figure 6 in the Nyquist representation, using frequency as an implicit variable. In order to calculate lifetime and mobility of charge carriers, we fitted the experimental data using a model based on the equivalent circuit depicted in the inset of Figure 6 (electrochemical impedance spectrum analyzer software for equivalent circuit modeling). In this model R_s accounts for the device series resistance, while R_{rec} represents the recombination resistance, related to the recombination current, C_μ is the chemical capacitance, due to the accumulation of photogenerated charge carriers, R_t represents the transport resistance, and C_g represents the geometrical capacitance of the device. The resulting effective lifetime of charge carriers ($\tau = R_{rec} \times C_\mu$) as well as the charge carrier mobility ($\mu = eD/kT$, where $D = L^2/(R_t \times C_\mu)$) are $\tau = 5.06 \times 10^{-5}$ s and $\mu = 4.28 \times 10^{-4}$ cm^2 V^{-1} s^{-1}, respectively.

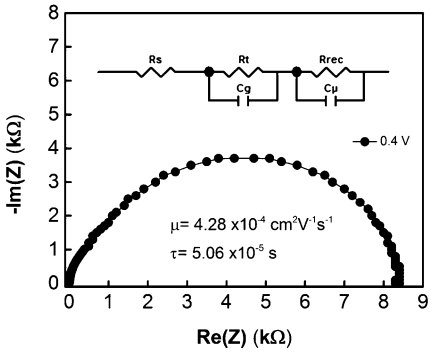

Figure 6. Impedance spectra of CZTS solar cells at applied biases of 0.4 V in the dark. Inset represents the equivalent circuit of the CZTS solar cell.

In order to confirm the results from impedance spectroscopy, we applied the photoinduced charge carrier extraction by linearly increasing voltage technique (photo-CELIV).[28] Photo-CELIV measurements have been introduced in the past to study the time-dependent charge carrier dynamics and concentration of photogenerated charge carriers of organic and inorganic semiconductor devices.[29] Further experimental details on the photo-CELIV measurements are given in the Supporting Information. The calculated average mobility of holes and electrons on the order of 1.30×10^{-4} cm^2 V^{-1} s^{-1} (Figure S5) resembles the value obtained from impedance spectroscopy. This charge carrier mobility matches values reported in the literature for CuInS (CIS) nanocrystal based solar cells,[30] but falls short compared to bulk CZTS based devices, which typically feature mobilities >1 cm^2 V^{-1} s^{-1}.[18] We emphasize that the results from photo-CELIV and impedance spectroscopy reflect the behavior of the complete CZTS solar cell, including the CdS layer. As such, it is not possible to directly elucidate the reason for the relatively low charge carrier mobility, since it could originate from the active layer or from

DOI: 10.1021/acsami.5b04468
ACS Appl. Mater. Interfaces 2015, 7, 21100−21106

any of the interfaces. However, a plausible explanation that emerges from our morphological data is the observation of small, low-crystalline domains and rather high porosity of the active layer providing an abundant surface area (Figures 2a,b and 3). The relatively low crystallinity and large surface area as compared to high-temperature CZTS (typically micrometer-sized domains) could explain the relatively low charge carrier mobility.

Additionally, from the photo-CELIV measurements we extracted the charge carrier concentration as a function of the delay time (Figure S5). This allows us to study the recombination behavior of charge carriers in low-temperature CZTS devices. Again, the extracted effective bimolecular lifetime (τ_B) of 3.28×10^{-5} s is in good agreement with the value obtained from our impedance measurements.

CONCLUSION

In conclusion, we present a novel and simple process to produce low-temperature sintered CZTS nanocrystal thin films using a rapid (5 min) annealing step. We verified the formation of the kesterite phase through XRD, Raman, and band gap measurements at temperatures below 350 °C. The fabricated solar cells based on low-temperature CZTS thin films exhibited a champion PCE of up to 1.85% with a photocurrent density of 8.57 mA/cm^2 for an absorber thickness of only 110 nm. On the basis of impedance spectroscopy and photo-CELIV measurements, we found that the mobility is one important factor limiting the performance of this type of device. A key advantage of our approach is the possibility to form a fused morphology without relying on high-temperature post-treatment or postsynthetic ligand exchange steps. The method presented here can serve as a universal approach for fabricating CZTS layers at relatively low temperatures with possible applications spanning from photovoltaics to thermoelectrics and photoelectrochemical devices. Future work should establish possible connections between morphology and device performance as suggested by our findings. Device engineering including electronically suitable buffer layers could be a promising route to further increase the efficiency of low-temperature CZTS films.

ASSOCIATED CONTENT

Supporting Information

The Supporting Information is available free of charge on the ACS Publications website at DOI: 10.1021/acsami.5b04468.

Experimental details, Figures S1−S5, and Table S1 (PDF)

AUTHOR INFORMATION

Corresponding Authors

*E-mail: yi.hou@fau.de.
*E-mail: hamed.azimi@fau.de.

Notes

The authors declare no competing financial interest.

ACKNOWLEDGMENTS

The authors would like to acknowledge the funding of the Deutsche Forschungsgemeinschaft (DFG) through the Cluster of Excellence Engineering of Advanced Materials, BAYER Technology Services, and the Energy Campus Nürnberg (ProjektSolarfabrik der Zukunft) for financial support. M.S. acknowledges primary support from a fellowship by the Portuguese Fundaçãopara a Ciência e a Tecnologia (SFRH/BPD/71816/2010) and the Erlangen Graduate School in Advanced Optical Technologies (SAOT) at the University of Erlangen—Nuremberg, which is funded by the German Research Foundation (DFG) within the framework of its "Excellence Initiative". The authors also acknowledge the support of Solar Technologies go Hybrid (SolTech) project from Bavarian Ministry of Science and Gradko International.

REFERENCES

(1) Akhavan, V. A.; Goodfellow, B. W.; Panthani, M. G.; Steinhagen, C.; Harvey, T.; Stolle, C. J.; Korgel, B. A. Colloidal CIGS and CZTS Nanocrystals: A Precursor Route to Printed Photovoltaics. *J. Solid State Chem.* **2012**, *189*, 2−12.

(2) Tian, Q.; Xu, X.; Han, L.; Tang, M.; Zou, R.; Chen, Z.; Yu, M.; Yang, J.; Hu, J. Hydrophilic Cu_2ZnSnS_4 Nanocrystals for Printing Flexible, Low-Cost and Environmentally Friendly Solar Cells. *CrystEngComm* **2012**, *14*, 3847−3850.

(3) Steinhagen, C.; Panthani, M. G.; Akhavan, V.; Goodfellow, B.; Koo, B.; Korgel, B. A. Synthesis of Cu_2ZnSnS_4 Nanocrystals for Use in Low-Cost Photovoltaics. *J. Am. Chem. Soc.* **2009**, *131*, 12554−12555.

(4) Steinhagen, C.; Harvey, T.; Stolle, C. J.; Harris, J. T.; Korgel, B. A. Pyrite Nanocrystal Solar Cells: Promising, or Fool's Gold? *J. Phys. Chem. Lett.* **2012**, *3*, 2352−2356.

(5) Tang, J.; Kemp, K. W.; Hoogland, S.; Jeong, K. S.; Liu, H.; Levina, L.; Furukawa, M.; Wang, X.; Debnath, R.; Cha, D.; et al. Colloidal-Quantum-Dot Photovoltaics Using Atomic-Ligand Passivation. *Nat. Mater.* **2011**, *10*, 765−771.

(6) Jeon, N. J.; Noh, J. H.; Yang, W. S.; Kim, Y. C.; Ryu, S.; Seo, J.; Seok, S. I. Compositional Engineering of Perovskite Materials for High-Performance Solar Cells. *Nature* **2015**, *517*, 476−480.

(7) Azimi, H.; Kuhri, S.; Osvet, A.; Matt, G.; Khanzada, L. S.; Lemmer, M.; Luechinger, N. A.; Larsson, M. I.; Zeira, E.; Guldi, D. M. Effective Ligand Passivation of Cu_2O Nanoparticles through Solid-State Treatment with Mercaptopropionic Acid. *J. Am. Chem. Soc.* **2014**, *136*, 7233−7236.

(8) Salvador, M.; Vorpahl, S. M.; Xin, H.; Williamson, W.; Shao, G.; Karatay, D. U.; Hillhouse, H. W.; Ginger, D. S. Nanoscale Surface Potential Variation Correlates with Local S/Se Ratio in Solution-Processed CZTSSe Solar Cells. *Nano Lett.* **2014**, *14*, 6926−6930.

(9) Ki, W.; Hillhouse, H. W. Earth-Abundant Element Photovoltaics Directly from Soluble Precursors with High Yield Using a Non-Toxic Solvent. *Adv. Energy Mater.* **2011**, *1*, 732−735.

(10) Todorov, T. K.; Reuter, K. B.; Mitzi, D. B. High-Efficiency Solar Cell with Earth-Abundant Liquid-Processed Absorber. *Adv. Mater.* **2010**, *22*, E156−E159.

(11) Guo, Q.; Ford, G. M.; Yang, W. C.; Walker, B. C.; Stach, E. A.; Hillhouse, H. W.; Agrawal, R. Fabrication of 7.2% Efficient CZTSSe Solar Cells Using CZTS Nanocrystals. *J. Am. Chem. Soc.* **2010**, *132*, 17384−17386.

(12) Azimi, H.; Hou, Y.; Brabec, C. J. Towards Low-Cost, Environmentally Friendly Printed Chalcopyrite and Kesterite Solar Cells. *Energy Environ. Sci.* **2014**, *7*, 1829−1849.

(13) Persson, C. Electronic and Optical Properties of Cu_2ZnSnS_4 and $Cu_2ZnSnSe_4$. *J. Appl. Phys.* **2010**, *107*, 053710.

(14) Jiang, C.; Lee, J. S.; Talapin, D. V. Soluble Precursors for $CuInSe_2$, $CuIn_{1-x}Ga_xSe_2$, and $Cu_2ZnSn(S,Se)_4$ Based on Colloidal Nanocrystals and Molecular Metal Chalcogenide Surface Ligands. *J. Am. Chem. Soc.* **2012**, *134*, 5010−5013.

(15) Cao, Y.; Denny, M. S.; Casper, J. V.; Farneth, W. E.; Guo, Q.; Ionkin, A. S.; Johnson, L. K.; Lu, M.; Malajovich, I.; Radu, D.; et al. High Efficiency Solution-Processed CZTSSe Thin Film Solar Cells Prepared from Binary and Ternary Nanoparticles. *J. Am. Chem. Soc.* **2012**, *134*, 15644−15647.

(16) Aldakov, D.; Lefrançois, A.; Reiss, P. Ternary and Quaternary Metal Chalcogenide Nanocrystals: Synthesis, Properties and Applications. *J. Mater. Chem. C* **2013**, *1*, 3756−3776.

DOI: 10.1021/acsami.5b04468
ACS Appl. Mater. Interfaces 2015, 7, 21100−21106

(17) Sun, Y.; Zhang, Y.; Wang, H.; Xie, M.; Zong, K.; Zheng, H.; Shu, Y.; Liu, J.; Yan, H.; Zhu, M. Novel Non-Hydrazine Solution Processing of Earth-Abundant $Cu_2ZnSn(S,Se)_4$ Absorbers for Thin-Film Solar Cells. *J. Mater. Chem. A* **2013**, *1*, 6880−6887.
(18) Shin, B.; Gunawan, O.; Zhu, Y.; Bojarczuk, N. A.; Chey, S. J.; Guha, S. Thin Film Solar Cell with 8.4% Power Conversion Efficiency Using An Earth-Abundant Cu_2ZnSnS_4 Absorber. *Prog. Photovoltaics* **2013**, *21*, 72−74.
(19) Shi, L.; Pei, C.; Xu, Y.; Li, Q. Template-Directed Synthesis of Ordered Single-Crystalline Nanowires Arrays of Cu_2ZnSnS_4 and $Cu_2ZnSnSe_4$. *J. Am. Chem. Soc.* **2011**, *133*, 10328−10331.
(20) Shavel, A.; Cadavid, D.; Ibáñez, M.; Carrete, A.; Cabot, A. Continuous Production of Cu_2ZnSnS_4 Nanocrystals in a Flow Reactor. *J. Am. Chem. Soc.* **2012**, *134*, 1438−1441.
(21) Singh, A.; Geaney, H.; Laffir, F.; Ryan, K. M. Colloidal Synthesis of Wurtzite Cu_2ZnSnS_4 Nanorods and Their Perpendicular Assembly. *J. Am. Chem. Soc.* **2012**, *134*, 2910−2913.
(22) Patterson, A. The Scherrer Formula for X-Ray Particle Size Determination. *Phys. Rev.* **1939**, *56*, 978−982.
(23) Walsh, A.; Chen, S.; Wei, S. H.; Gong, X. G. Kesterite Thin-Film Solar Cells: Advances in Materials Modelling of Cu_2ZnSnS_4. *Adv. Energy Mater.* **2012**, *2*, 400−409.
(24) Nanu, M.; Schoonman, J.; Goossens, A. Nanocomposite Three-Dimensional Solar Cells Obtained by Chemical Spray Deposition. *Nano Lett.* **2005**, *5*, 1716−1719.
(25) Bisquert, J.; Bertoluzzi, L.; Mora-Sero, I.; Garcia-Belmonte, G. Theory of Impedance and Capacitance Spectroscopy of Solar Cells with Dielectric Relaxation, Drift-Diffusion Transport, and Recombination. *J. Phys. Chem. C* **2014**, *118*, 18983−18991.
(26) Fabregat-Santiago, F.; Garcia-Belmonte, G.; Mora-Seró, I.; Bisquert, J. Characterization of Nanostructured Hybrid and Organic Solar Cells by Impedance Spectroscopy. *Phys. Chem. Chem. Phys.* **2011**, *13*, 9083−9118.
(27) Garcia-Belmonte, G.; Guerrero, A.; Bisquert, J. Elucidating Operating Modes of Bulk-Heterojunction Solar Cells from Impedance Spectroscopy Analysis. *J. Phys. Chem. Lett.* **2013**, *4*, 877−886.
(28) Pivrikas, A.; Sariciftci, N.; Juška, G.; Österbacka, R. A Review of Charge Transport and Recombination in Polymer/Fullerene Organic Solar Cells. *Prog. Photovoltaics* **2007**, *15*, 677−696.
(29) Juška, G.; Arlauskas, K.; Viliūnas, M.; Kočka, J. Extraction Current Transients: New Method of Study of Charge Transport in Microcrystalline Silicon. *Phys. Rev. Lett.* **2000**, *84*, 4946−4949.
(30) Azimi, H.; Heumüller, T.; Gerl, A.; Matt, G.; Kubis, P.; Distaso, M.; Ahmad, R.; Akdas, T.; Richter, M.; Peukert, W.; Brabec, C. J. Relation of Nanostructure and Recombination Dynamics in a Low-Temperature Solution-Processed $CuInS_2$Nanocrystalline Solar Cell. *Adv. Energy Mater.* **2013**, *3*, 1589−1596.

DOI: 10.1021/acsami.5b04468
ACS Appl. Mater. Interfaces 2015, 7, 21100−21106